Experimental and Theoretical Investigations of the Stability of Two Small Gaseous Dicarboxylate Dianions: Acetylene Dicarboxylate and Succinate

Piotr Skurski,[†,§] Jack Simons,*[,†] Xue-Bin Wang,[‡] and Lai-Sheng Wang*[,‡]

Contribution from the Department of Chemistry, University of Utah, Salt Lake City, Utah 84112, Department of Physics, Washington State University, 2710 University Drive, Richland, Washington 99352, and W. R. Wiley Environmental Molecular Sciences Laboratory, Pacific Northwest National Laboratory, MS K8-88, P.O. Box 999, Richland, Washington 99352

Received February 1, 2000

Abstract: The stability of two small dicarboxylate dianions, $(O_2C-C\equiv C-CO_2)^{2-}$ (AD^{2-}) and $(O_2C-CH_2-CH_2-CO_2)^{2-}$ (SD^{2-}) has been studied in the gas phase by using electrospray mass spectrometry, photoelectron spectroscopy, and ab initio calculations. Despite their similar charge-separation and size, AD^{2-} was observed abundantly, whereas SD^{2-} was very difficult to detect. Our ab initio calculation predicts that AD^{2-} is adiabatically stable with respect to electron loss whereas SD^{2-} is not. These calculations show that AD^{2-} has a D_{2d} structure with 0.418 eV adiabatic and 0.69 eV vertical electron binding energies, compared to the experimental values of 0.30 (0.10) and 0.60 (0.10) eV, respectively. SD^{2-} was found to have a C_{2h} structure with a negative adiabatic electron binding energy (−0.086 eV). Our detailed theoretical analysis indicates that while the two excess charges in SD^{2-} are completely localized on the terminal carboxylate groups, there is significant delocalization of the excess charges into the −CC− π-type orbitals in AD^{2-}. The D_{2d} structure of the AD^{2-} dianion allows each carboxylate to interact with one of the two perpendicular π-type orbitals of the acetylene moiety, thus providing extra stabilization while minimizing the Coulomb repulsion.

1. Introduction

Despite their ubiquity in the condensed phase, our knowledge about free multiply charged anions (MCAs) remains quite scarce until recently.[1−17] The strong Coulomb repulsion between the excess charges limits only a few neutral molecules to bind more than one extra electron. Generally MCAs are expected to occur for relatively large molecular systems, where the Coulomb repulsion among the excess charges is reduced. On the other hand, specific molecular properties, such as the details of the molecular and electronic structures, should also be important in determining the stability of an MCA, but have not been extensively explored and understood well. Thus it is desirable and illuminating to compare MCAs which have similar molecular size, geometrical structure, and compositions, yet display different stability.

The electronic and thermodynamic stabilities of a number of small dianions have been investigated theoretically.[7−17] Several dianionic species have been predicted to be electronically stable in the gas phase. However, experimental investigations of MCAs have been especially challenging primarily due to the difficulty of making these species in isolated forms and in sufficient quantity for experimental interrogations.[1−6] Recently, we have developed a new experimental technique to investigate gas-phase MCAs using photodetachment photoelectron spectroscopy (PES) and electrospray ionization.[18−20] PES is particularly ideal to probe the intrinsic properties of free MCAs and directly yields

† University of Utah.

§ Permanent address: University of Gdañsk, Department of Chemistry, 80−952 Gdañsk, Poland.

‡ Washington State University and Pacific Northwest National Laboratory.

(1) Compton, R. N. Negative Ion States. In *Photophysics and Photochemistry in the Vacuum. Ultraviolet*; McGlynn, S. P., et al., Eds.; Reidel: The Netherlands, 1985.

(2) Kalcher, J.; Sax, A. F. *Chem. Rev.* **1994**, *94*, 2291.

(3) Scheller, M. K.; Compton, R. N.; Cederbaum, L. S. *Science* **1995**, *270*, 1160.

(4) Freeman, G. R.; March, N. H. *J. Phys. Chem.* **1996**, *100*, 4331.

(5) Schauer, S. N.; Williams, P.; Compton, R. N. *Phys. Rev. Lett*. **1990**. *65*, 625. Jin, C.; Hettich, R. L.; Compton, R. N.; Tuinman, A. A.; Derecskei-Kovacs, A.; Marynick, D. S.; Dunlap, B. I. *Phys. Rev. Lett.* **1994**, *73*, 2821.

(6) Compton, R. N.; Tuinman, A. A.; Klots, C. E.; Pederson, M. R.; Patton, D. C. *Phys. Rev. Lett.* **1997**, *78*, 4367.

(7) Scheller, M. K.; Cederbaum, L. S. *J. Chem. Phys*. **1993**, *99*, 441. Scheller, M. K.; Cederbaum, L. S. *J. Chem. Phys*. **1994**, *100*, 8934.

(8) Sommerfeld, T.; Scheller, M. K.; Cederbaum, L. S. *J. Chem. Phys*. **1995**, *103*, 1057. Weikert, H. G.; Meyer, H. D.; Cederbaum, L. S. *J. Chem. Phys*. **1996**, *104*, 7122.

(9) Dreuw, A.; Sommerfeld, T.; Cederbaum, L. S. *J. Chem. Phys*. **1998**, *109*, 2727.

(10) Zakrzewski, V. G.; Ortiz, J. V. *J. Chem. Phys*. **1995**, *102*, 294. Enlow, M.; Ortiz, J. V.; Luthi, H. P. *Mol. Phys*. **1997**, *92*, 441. Dolgounitcheva, O.; Zakrzewski, V. G.; Ortiz, J. V. *J. Chem. Phys*. **1998**, *109*, 87.

(11) Boldyrev, A. I.; Simons, J. *J. Chem. Phys*. **1992**, *97*, 2826. Boldyrev, A. I.; Simons, J. *J. Chem. Phys*. **1993**, *98*, 4745. Boldyrev, A. I.; Simons, J. *J. Phys. Chem*. **1994**, *98*, 2293.

(12) Gutowski, M.; Boldyrev, A. I.; Ortiz, J. V.; Simons, J. *J. Am. Chem. Soc*. **1994**, *116*, 9262.

(13) Gutowski, M.; Boldyrev, A. I.; Simons, J.; Rak, J.; Blazejowski, J. *J. Am. Chem. Soc*. **1996**, *118*, 1173.

(14) Boldyrev, A. I.; Gutowski, M.; Simons, J. *Acc. Chem. Res*. **1996**, *29*, 497.

(15) Stefanovich, E. V.; Boldyrev, A. I.; Truong, T. N.; Simons, J. *J. Phys. Chem*. B. **1998**, *102*, 4205.

(16) Adamowicz, L. *J. Chem. Phys*. **1991**, *95*, 8669. Watts, J. D.; Bartlett, R. J. *J. Chem. Phys*. **1992**, *97*, 3445. Zakrzewski, V. G.; Ortiz, J. V. *J. Chem. Phys*. **1995**, *102*, 294. Enlow, M.; Ortiz, J. V.; Luthi, H. P. *Mol. Phys*. **1997**, *92*, 441. Dolgounitcheva, O.; Zakrzewski, V. G.; Ortiz, J. V. *J. Chem. Phys*. **1998**, *109*, 87.

(17) Gronert, S. *Int. Mass. Spectrom*. **1999**, *185−187*, 351. Flores, A. E.; Gronert, S. *J. Am. Chem. Soc*. **1999**, *121*, 2627.

10.1021/ja000371f CCC: $19.00
Published on Web 04/15/2000

information about their electronic stability, intramolecular Coulomb repulsion, and solvation effects. This technique is particularly sensitive and powerful to allow a broad range of MCAs that exist in solution to be interrogated for the first time in the gas phase.[19−30]

One particularly important class of dianions is the organic dicarboxylates, which exist in aqueous solutions as a result of dissociation of the parent organic diacids. These species are quite interesting in that their excess charges are localized on the carboxylate groups, allowing the electrostatic interactions to be understood straightforwardly. We have investigated, using PES, the stability and intramolecular Coulomb repulsion in a series of such dianions with saturated carbon backbones, $^{-}O_2C-(CH_2)_n-CO_2^{-}$ ($n = 3-10$).[21−24] However, we failed to obtain the PES spectrum of the dianion with $n = 2$ (succinate) owing to difficulties in observing this species using our electrospray source.[22] We rationalized qualitatively that the strong Coulomb repulsion in this small molecular dianion makes it unstable or short-lived in the gas phase, although it had been observed previously in a collisionally induced "ion pair" formation process.[31] However, its absolute electronic or thermodynamic stability in the gas phase remained unknown. Surprisingly, we were able to observe abundantly a dianion, acetylene dicarboxylate (AD^{2-}), $^{-}O_2C-C\equiv C-CO_2^{-}$, which has a similar size as the succinate dianion (SD^{2-}), $^{-}O_2C-CH_2CH_2-CO_2^{-}$, that was extremely difficult to detect. Although the C≡C triple bond may allow charge delocalization, we did not expect this to be necessarily favorable in the dianion because charge delocalization can lead to *enhanced* Coulomb repulsion between the two electrons on the $-CO_2^{-}$ termini. So the question we wanted to address is what determines the electronic stabilities of these two dianions and what accounts for their different stabilities?

In this article, we present a detailed ab initio study on these two small dianions and compare the theoretical results with experimental observations. We obtained the PES spectra of AD^{2-} at three photon energies, 355, 266, and 193 nm. AD^{2-} was determined to be electronically stable with a 0.30 (0.10) eV adiabatic electron binding energy and a 0.60 (0.10) eV vertical electron binding energy. Numerous photodetachment features, due to excited states of the AD^{-} monoanion, were also observed. Our ab initio study indicates indeed that AD^{2-} is adiabatically stable with respect to electron loss whereas SD^{2-} is not. Detachment channels from AD^{2-} to various states of AD^{-} were calculated and compared to the experimental observations. We found that AD^{2-} has a D_{2d} structure, in which the two $-CO_2^{-}$ groups are perpendicular to each other. This structure allows the negative charge on each terminal carboxylate group to partially delocalize to each of the two perpendicular π-type orbitals of the C≡C triple bond, thereby giving a slight enhancement of electronic stability, even though the Coulomb repulsion may be slightly increased by such delocalization. In contrast, we found that SD^{2-} has a C_{2h} structure with the two charges completely localized on the terminal $-CO_2^{-}$ groups because delocalization is not possible in this species. We therefore conclude that delocalization into the −CC− π-type orbitals provides the extra electronic stability for AD^{2-} relative to SD^{2-}.

2. Experimental Methods

The experiments were carried out with a photodetachment spectroscopy facility that involves a magnetic-bottle time-of-flight photoelectron analyzer and an electrospray ion source. Details of the apparatus have been published previously[18] and only a brief description is given here. To produce the desired dianions, we used a 5×10^{-4} molar solution of the corresponding diacids (acetylene dicarboxylic acid, HOOC−C≡C−COOH and succinic acid, HOOC−CH_2CH_2−COOH) under a basic condition (by adding NaOH) in a water/methanol mixed solvent (10/90 volume ratio). Each solution was sprayed through a 0.01-mm diameter syringe needle at ambient atmosphere and at a high voltage bias of −2.2 kV, producing highly charged liquid droplets, which were fed into a desolvation capillary. Negatively charged molecular ions emerging from the desolvation capillary were guided by a radio frequency-only quadrupole ion guide into a 3-D quadrupole ion trap, where the ions were accumulated for 0.1 s before being pushed into the extraction zone of a time-of-flight mass spectrometer. The major anions from the acetylene dicarboxylic acid solution were the totally deprotonated AD^{2-} dianion and its monoprotonated anion, HOOC−C≡C−COO^{-}. For the succinic acid solution, we were only able to observe abundantly the monoprotonated species, HOOC−CH_2CH_2−COO^{-}. The desired totally deprotonated dianion (SD^{2-}) was very difficult to observe. It was present only with extremely weak abundance, and hence we were not able to obtain its PES spectrum.

In the PES experiment, the AD^{2-} dianions were mass selected and decelerated before being intercepted by a laser beam in the detachment zone of the magnetic-bottle photoelectron analyzer. Both an Nd:YAG laser (355 and 266 nm) and an excimer laser (193 nm) were used for photodetachment. Photoelectron time-of-flight spectra were collected at nearly 100% efficiency by the magnetic bottle and then converted to kinetic energy spectra, calibrated by the known spectra of I^{-} and O^{-}. The binding energy spectra were obtained by subtracting the kinetic energy spectra from the photon energy. The electron kinetic energy resolution was $\Delta E/E \sim 2\%$, i.e., 20 meV for 1 eV electrons.

3. Theoretical Methods

The equilibrium geometries of the neutral and anionic species were optimized and their harmonic vibrational frequencies calculated at the second-order Møller−Plesset (MP2) perturbation theory level. In all calculations, the values of $<S^2>$ never exceeded 2.03 for triplets and 0.78 for doublet states, so we are confident that spin-contamination effects were not serious. The electronic stabilities of the anions in their ground states were calculated using a supermolecular approach (i.e., by subtracting the energies of the $(n + 1)$-electron species from those of the n-electron systems). This approach requires the use of size-extensive methods, so we employed Møller−Plesset perturbation theory up to fourth order as well as the coupled-cluster method with single, double, and noniterative triple excitations (CCSD(T)).[32,33] In addition, the electron binding energies were analyzed within the perturbation framework, which generates Koopmans' theorem (KT),[34] SCF-differ-

(18) Wang, L. S.; Ding, C. F.; Wang, X. B.; Barlow, S. E. *Rev. Sci. Instrum.* **1999**, *70*, 1957.
(19) Wang, L. S. *Comments At. Mol. Phys.* **2000**, in press.
(20) Wang, L. S.; Wang, X. B. *J. Phys. Chem.* A **2000**, *104*, 1978.
(21) Wang, X. B.; Ding, C. F.; Wang, L. S. *Phys. Rev. Lett.* **1998**, *81*, 3351.
(22) Wang, L. S.; Ding, C. F.; Wang, X. B.; Nicholas, J. B. *Phys. Rev. Lett.* **1998**, *81*, 2667.
(23) Ding, C. F.; Wang, X. B.; Wang, L. S. *J. Phys. Chem.* A **1998**, *102*, 8633.
(24) Wang, X. B.; Ding, C. F.; Wang, L. S. *Chem. Phys. Lett.* **1999**, *307*, 391.
(25) Ding, C. F.; Wang, X. B.; Wang, L. S. *J. Chem. Phys.* **1999**, *110*, 3635. Wang, X. B.; Ding, C. F.; Nicholas, J. B.; Dixon, D. A.; Wang, L. S. *J. Phys. Chem.* A **1999**, *103*, 3423.
(26) Wang, X. B.; Wang, L. S. *J. Chem. Phys.* **1999**, *111*, 4497.
(27) Wang, X. B.; Wang, L. S. *Nature* **1999**, *400*, 245. Wang, X. B.; Ferris, K.; Wang, L. S. *J. Phys. Chem.* A **2000**, *104*, 25.
(28) Wang, X. B.; Wang, L. S. *Phys. Rev. Lett.* **1999**, *83*, 3402.
(29) Wang, X. B.; Wang, L. S. *J. Am. Chem. Soc.* **2000**, *122*, 2096, 2339.
(30) Wang, X. B.; Wang, L. S. *J. Phys. Chem. A.* **2000**, *104*, in press.
(31) Maas, W. P. M.; Nibbering, N. M. M. *Int. J. Mass Spectrom. Ion Processes* **1989**, *88*, 257.
(32) Bartlett, R. J.; Stanton, J. F. In *Reviews in Computational Chemistry*; Lipkowitz, K. B., Boyd, D. B., Eds.; VCH Publishers: New York, 1994; Vol. V.
(33) Taylor, P. R. In *Lecture Notes in Quantum Chemistry II*; Roos, B. O., Ed.; Springer-Verlag: Berlin, 1994.
(34) Koopmans, T. *Physica (Amsterdam)* **1934**, *1*, 104.

ence (ΔSCF), Møller−Plesset difference (MP*n*), and coupled-cluster difference values of the binding energies. For studying the bound excited states of the AD^- monoanion, we also used the restricted outer valence Green's function (OVGF) method[35−37] followed by CCSD(T) estimations. All calculations were performed with the GAUSSIAN 98 program[38] on 500-MHz dual processor Intel Pentium III computers and on an SGI Origin2000 numerical server. The three-dimensional plots of molecular orbitals were generated with the MOLDEN program.[39]

The choice of the atomic orbital basis sets used to describe the neutral molecules and the excess bound electrons is very important for reproducing the correct value of electron binding energies. The basis sets must be flexible enough to describe the static charge distribution of the neutral molecular host and to allow for polarization and dispersion stabilization of the anions upon electron attachment. On the basis of extensive earlier experience on anions and dianions, we decided to use the aug-cc-pVDZ basis set[40] for optimizing the geometries and calculating vibrational frequencies and to employ the aug-cc-pVDZ+2s2p basis (supplemented with diffuse functions) for calculating electron binding energies. The addition of extra diffuse functions with low exponents was necessary especially to describe more properly the dianions' pair of excess electrons. In particular, we supplemented the aug-cc-pVDZ basis set with extra even-tempered[41] two-term s and two-term p sets of diffuse functions centered on both C atoms in the CO_2 groups. The extra diffuse s and p functions do not share exponent values and the geometric progression ratio was equal to 3.2,[42] and for every symmetry, we started to build up the exponents from the lowest exponent included in the aug-cc-pVDZ basis set designed for carbon. As a consequence, we achieved lowest exponents of 4.580078×10^{-5} and 3.946289×10^{-5} au for s and p symmetry, respectively. Finally, the atomic partial charges calculated in this work were fit to the electrostatic potential (ep) according to the Merz−Singh−Kollman scheme.[43]

4. Experimental Results

4.1. Photoelectron Spectra of $^-O_2C-C\equiv C-CO_2^-$ (AD^{2-}). The PES spectra of the AD^{2-} dianion are shown in Figure 1 at three detachment photon energies. The 193-nm spectrum (Figure 1c) revealed five distinct detachment bands between 0.3 and 2.8 eV, labeled as X and A−D. At 266 nm (Figure 1b), the C and D bands disappeared almost completely, despite the fact that the 266-nm photon energy is higher than the binding energies of these two bands. In addition, the relative intensity of the B-band was observed to be reduced at 266 nm. At 355 nm (Figure 1a), the B-band almost completely disappeared, whereas the relative intensity of the A-band was reduced. Furthermore, the A-band was slightly shifted to a lower binding energy. The sequential disappearance of PES features at low

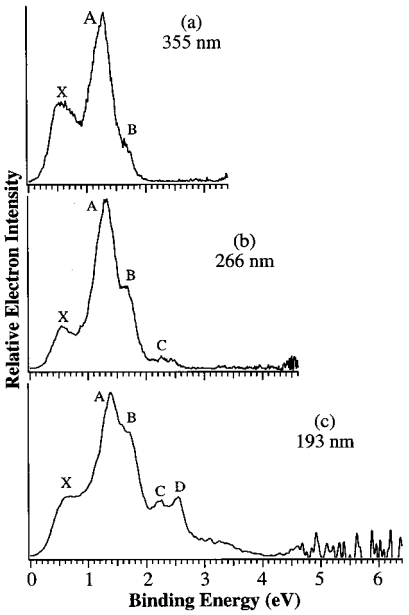

Figure 1. Photoelectron spectra of $(O_2C-C\equiv C-CO_2)^{2-}$ at (a) 355 (3.496 eV), (b) 266 (4.661 eV), and (c) 193 nm (6.424 eV).

detachment photon energies is characteristic of photodetachment of MCAs, and it is a direct consequence of the repulsive Coulomb barrier (RCB) that exists in MCAs against electron detachment. From the photon-energy-dependent PES spectra, we can estimate the magnitude of the RCB in AD^{2-}, as will be shown below.

The PES features in Figure 1 represent photodetachment transitions from the electronic ground state of AD^{2-} to the ground and excited states of the corresponding singly charged anion (AD^-). Within Koopmans' approximation, these features can be alternatively viewed as removing electrons from the occupied molecular orbitals (MOs) of AD^{2-}. The threshold of the PES spectra yields the adiabatic binding energy of the second excess electron in AD^{2-}, or the second electron affinity of the AD neutral. Due to the broad nature of the X-band, we can only obtain an estimate of the adiabatic binding energy of AD^{2-} as 0.30 (0.10) eV with a relatively large uncertainty. The vertical binding energy of the second electron in AD^{2-}, representing the energy difference between the ground states of AD^{2-} and AD^- at the equilibrium geometry of AD^{2-}, was measured to be 0.60 (0.10) eV. The X-band represents the transition from the ground state of AD^{2-} to that of AD^-, its great width indicates large equilibrium geometry changes between the ground states of AD^{2-} and AD^-.

The higher binding energy features (A−D), which may contain overlapping electronic transitions, represent removal of more tightly bound electrons from AD^{2-}, which thus produces excited states of AD^-. The canonical vertical detachment energies of these features are given in Table 1, where they are compared to theoretical calculations, as will be discussed later.

4.2. Photon-Energy-Dependent PES Spectra and the Repulsive Coulomb Barrier. As we reported previously, there is an essential difference between photodetachment of multiply and singly charged anions. When an electron is removed from an MCA, the two photoproducts, a free electron and an anion with one less charge than the parent MCA, are both negatively charged. The superposition of the long-range Coulomb repulsion between the outgoing electron and the remaining anion and the short-range electron binding produces an effective potential barrier for the outgoing electron. Thus one has an interesting situation, where, if the detachment photon energy is below the

(35) Ortiz, J. V. *J. Chem. Phys.* **1988**, *89*, 6348.
(36) Cederbaum, L. S. *J. Phys.* **1975**, *B8*, 290.
(37) Zakrzewski, V. G.; von Niessen, W. *J. Comput. Chem.* **1993**, *14*, 13.
(38) GAUSSIAN 98, Revision A.7; Frisch, M. J.; Trucks, G. W.; Schlegel, H. B.; Scuseria, G. E.; Robb, M. A.; Cheeseman, J. R.; Zakrzewski, V. G.; Montgomery, J. A., Jr.; Stratmann, R. E.; Burant, J. C.; Dapprich, S.; Millam, J. M.; Daniels, A. D.; Kudin, K. N.; Strain, M. C.; Farkas, O.; Tomasi, J.; Barone, V.; Cossi, M.; Cammi, R.; Mennucci, B.; Pomelli, C.; Adamo, C.; Clifford, S.; Ochterski, J.; Petersson, G. A.; Ayala, P. Y.; Cui, Q.; Morokuma, K.; Malick, D. K.; Rabuck, A. D.; Raghavachari, K.; Foresman, J. B.; Cioslowski, J.; Ortiz, J. V.; Baboul, A. G.; Stefanov, B. B.; Liu, G.; Liashenko, A.; Piskorz, P.; Komaromi, I.; Gomperts, R.; Martin, R. L.; Fox, D. J.; Keith, T.; Al-Laham, M. A.; Peng, C. Y.; Nanayakkara, A.; Gonzalez, C.; Challacombe, M.; Gill, P. M. W.; Johnson, B.; Chen, W.; Wong, M. W.; Andres, J. L.; Gonzalez, C.; Head-Gordon, M.; Replogle, E. S.; Pople, J. A. Gaussian, Inc.: Pittsburgh, PA, 1998.
(39) Schaftenaar, G. MOLDEN, CAOS/CAMM Center, The Netherlands, 1991.
(40) Kendall, R. A.; Dunning, T. H, Jr.; Harrison, R. J. *J. Chem. Phys.* **1992**, *96*, 6796.
(41) Schmidt, M. W.; Ruedenberg, K. *J. Chem. Phys.* **1979**, *71*, 3961.
(42) Gutowski, M.; Simons, J. *J. Chem. Phys.* **1990**, *93*, 3874.
(43) Besler, B. H.; Merz, K. M., Jr.; Kollman, P. A. *J. Comput. Chem.* **1990**, *11*, 431.

Table 1. Experimental and Theoretical Vertical Binding Energies (VDE in eV) of AD^{2-}

experimental		theoretical			
band	VDE	MO[a]	FS[b]	OVGF	CCST(D)
X	0.60 (0.10)	e	^2E	1.011	0.693
A	1.31 (0.10)	a_1	$^2A_1$	1.815	1.269
	1.31 (0.10)	a_2	$^2A_2$	1.934	1.445
	1.31 (0.10)	b_1	$^2B_1$	1.937	1.450
B	1.70 (0.10)	b_2	$^2B_2$	2.310	
C	2.20 (0.10)	e	^2E	2.476	
D	2.60 (0.10)				
		e	^2E	6.022	

[a] MO's from which an electron is removed. [b] Final state terms under the D_{2h} symmetry of AD^{2-}.

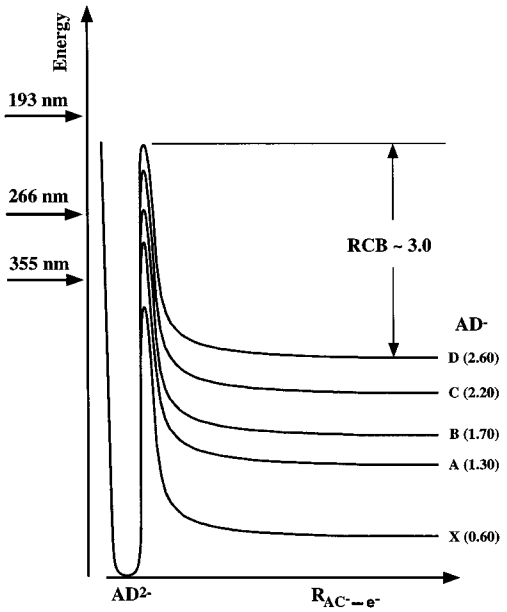

Figure 2. Schematic drawing of the potential energy curves showing the repulsive Coulomb barriers (RCB) of $(O_2C-C\equiv C-CO_2)^{2-}$ (AD^{2-}) with respect to the different final states of the singly charged anion (AD^-). The vertical binding energies and the estimated RCB are shown in eV. The relative positions of the three photon energies used are also indicated.

top of the RCB, no electron detachment will occur even if the photon energy is above the asymptotic electron binding energy (i.e., energetically and thermodynamically possible). In this case, detachment can only take place through electron tunneling, which depends exponentially on the distance between the photon energy and the RCB top and becomes negligible if the photon energy is far below the barrier top.[24] When the photon energy is around the RCB top, the detachment signal will be reduced.

The successive disappearance and reduction in relative peak intensities of the higher binding energy features at the lower photon energies in Figure 1 are direct consequences of the RCB. Figure 2 schematically illustrates the RCBs for removing electrons from AD^{2-}, leading to the different observed PES features. The relative positions of the three photon energies used and the vertical binding energies of all the observed features are also shown. Each detachment channel has its own RCB, which may have different magnitudes for large molecules if the detached electrons are from different parts of the molecules and thus experience slightly different Coulomb repulsion. If we assume that the RCB is the same for the different channels (a reasonable assumption for small molecules), we can estimate the magnitude of the RCB based on the photon energy dependence of appearance or disappearance of the PES features.

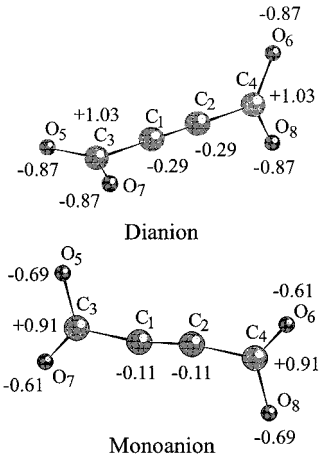

Figure 3. The minimum energy structures for $(O_2C-C\equiv C-CO_2)^{2-}$ (D_{2d}) and $(O_2C-C\equiv C-CO_2)^-$ (C_{2h}). The numbers are the ep charges.

Table 2. MP2 Geometries and Vibrational Frequencies Calculated for the Dianion and Monoanion of $(O_2C-CC-CO_2)$[a]

parameter	value	vibrational frequencies		
D_{2d} equilibrium structure of $(O_2C-CC-CO_2)^{2-}$				
$r(C_1C_2)$	1.248	$\nu_1(b_1) = 32$	$\nu_{2,3}(e) = 97$	$\nu_{4,5}(e) = 195$
$r(C_1C_3)$	1.504	$\nu_6(a_1) = 336$	$\nu_{7,8}(e) = 550$	$\nu_9(b_2) = 646$
$r(C_3O_5)$	1.274	$\nu_{10,11}(e) = 773$	$\nu_{12}(a_1) = 795$	$\nu_{13}(b_2) = 958$
$\alpha(O_5C_3O_7)$	127.884	$\nu_{14}(b_2) = 1310$	$\nu_{15}(a_1) = 1321$	$\nu_{16,17}(e) = 1596$
		$\nu_{18}(a_1) = 2180$		
C_{2h} equilibrium structure of $(O_2C-CC-CO_2)^-$				
$r(C_1C_2)$	1.250	$\nu_1(b_u) = 88$	$\nu_2(a_u) = 91$	$\nu_3(a_u) = 117$
$r(C_2C_3)$	1.461	$\nu_4(a_g) = 164$	$\nu_5(a_g) = 361$	$\nu_6(b_g) = 386$
$r(C_3O_5)$	1.238	$\nu_7(a_u) = 469$	$\nu_8(a_g) = 519$	$\nu_9(b_u) = 643$
$r(C_3O_7)$	1.302	$\nu_{10}(b_u) = 750$	$\nu_{11}(a_g) = 865$	$\nu_{12}(a_g) = 919$
$\alpha(O_5C_3O_7)$	129.345	$\nu_{13}(b_u) = 1041$	$\nu_{14}(b_u) = 1500$	$\nu_{15}(a_g) = 1635$
$\alpha(C_2C_1C_3)$	169.000	$\nu_{16}(b_u) = 1986$	$\nu_{17}(a_g) = 2083$	$\nu_{18}(a_g) = 3650$

[a] Distances in Å, valence (α) and dihedral (γ) angles in deg, frequencies in cm^{-1}. See Figure 3 for atom numbering.

Figure 1c showed that the spectrum seemed to be cut off just beyond the D-band, suggesting that the 193-nm photon energy was above the RCB of the D-band, i.e., RCB < ~3.8 eV (6.424 − 2.60 eV). The disappearance of the D-band at 266 nm (Figure 1b) suggested that the 266-nm photon was below the RCB of the D-band, i.e., RCB > 2.1 eV (4.661 − 2.60 eV). Furthermore, the relative intensity of the B-band was reduced at 266 nm, suggesting that the 266-nm photon was near the RCB top of the B-band. We inferred that the RCB should be ~3 eV (4.661 − 1.70 eV), which is just about the mean value from those derived from the D-band above (2.1 < RCB < 3.8 eV). As we have shown previously, the RCB is equal to the magnitude of the intramolecular Coulomb repulsion between the two excess charges.[22] We will show below that our derived RCB of ~3 eV is consistent with the intramolecular Coulomb repulsion in AD^{2-}, based on the theoretical structural parameters.

5. Theoretical Results

5.1. MP2 Geometries and Harmonic Frequencies of AD^{2-} and AD^-. Our investigation of the potential energy surfaces of neutral AD and its negative daughters resulted in a D_{2d} minimum energy structure for AD^{2-} and a C_{2h} minimum for AD^-. These structures are depicted in Figure 3 and characterized in detail in Table 2, where their vibrational frequencies are also reported. Even though the D_{2d} geometry corresponds to the lowest energy structure for AD^{2-}, it should be noted that the kinetic barrier for rotation around the −CC− bond (leading to a D_{2h} structure) is relatively small (0.040 eV at the MP2 level and 0.076 eV at

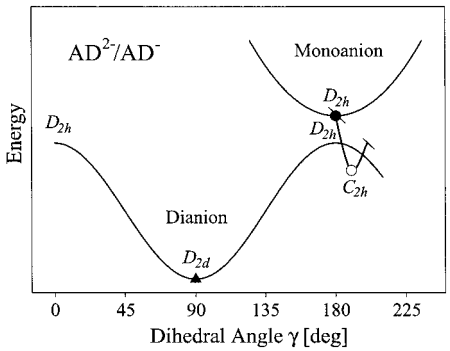

Figure 4. Schematic potential energy curves along the dihedral angle for $(O_2C-C\equiv C-CO_2)^{2-}$ and $(O_2C-C\equiv C-CO_2)^2$, showing the D_{2d} and D_{2h} minima of the dianion and monoanion, respectively. Note the true minimum for the monoanion has C_{2h} symmetry, which is schematically indicated.

Table 3. Electron Binding Energies (eV) for the Monoanion and Dianion of $(O_2C-CC-CO_2)$

	D_{2d} geometry of the dianion		C_{2h} geometry of the monoanion	
E	1st electron	2nd electron	1st electron	2nd electron
E^{KT}		2.232	–	1.116
E^{SCF}	4.164	0.727	2.282	−0.385
E^{MP2}	4.047	1.686	5.661	−0.364
E^{MP3}	4.171	1.587	4.683	−0.198
E^{MP4}	4.282	1.326	5.384	−0.384
$E^{CCSD(T)}$	4.745	0.693	4.967	−0.315
$E^{CCSD(T)}$ + ΔZPE		0.895		−0.113

the CCSD(T) level), as schematically shown in Figure 4. The corresponding potential energy profile for AD^- is also schematically shown in Figure 4, where we attempt to show that the minimum is not exactly D_{2h} but is slightly distorted and possesses the lower C_{2h} symmetry. The energy of the monoanion is higher than that of the dianion for every value of the dihedral angle γ, as long as the D-type symmetry is preserved. However, in the region of the monoanion's D_{2h} stationary point, deformation to C_{2h} symmetry causes the dianion to become electronically unstable (see also Table 3). Even though the dianion is not electronically stable for such C_{2h} configurations of the nuclei, AD^{2-} is adiabatically stable since the D_{2d} dianion's minimum lies below the C_{2h} monoanion's (see Figure 4).

Our calculations indicate that the attachment of the second electron leads to a slight increase in the C1−C3 and C2−C4 bond lengths (by 0.043 Å). Larger geometry changes occur in several valence and dihedral angles. In particular, the planarity of the monoanion that permits delocalization of the single negative charge over the two −COO groups is replaced by a nonplanar structure of the dianion, in which the two −COO groups become perpendicular to each other. These geometry differences can be understood based on the Coulomb repulsion within the dianion. The nonplanarity of AD^{2-} facilitates charge localization, allowing the two excess charges to be separated spatially. In the D_{2d} structure each of the −COO groups can interact with one component of the acetylene C−C π-type MOs (consisting of two perpendicular components). The increased charge on C1 and C2 in AD^{2-} compared to AD^- (Figure 3) is consistent with partial delocalization of the excess charges into the π-type MOs.

5.2. Electron Binding Energies of AD^- and AD^{2-}. The AD^{2-} dianion is an electronically bound closed-shell singlet $^1A_1$ system while the corresponding monoanion is an open-shell ^2E species at the D_{2d} symmetry of AD^{2-}. The electron binding energy was calculated at successive levels of theory (KT, SCF, MPn (n = 2, 3, 4), and CCSD(T)), and the results at the equilibrium geometries of the mono- and dianion are presented in Table 3.

Since our experiment involves photodetachment of one excess electron from the dianion, we emphasize the vertical binding energies for the dianionic D_{2d} geometry when comparing with our experimental findings. Our best theoretical estimation of the vertical detachment energy for AD^{2-} (calculated at the CCSD(T) level) is 0.693 eV, which is in good agreement with the VDE assigned to the X-band (0.60 eV), although addition of zero-point energy corrections weakens this agreement. Moreover, our calculated value of the adiabatic electron affinity (at the same level), 0.418 eV, agrees well with the experimental ADE of 0.30 eV.

In considering the D_{2d} binding energies reported in Table 3 at the various levels of theory, it should be noted that the stability of the dianion is overestimated in most methods, and that highly correlated calculations are needed to reproduce the correct value of electron binding energies. For example, we note that the MP perturbation series converges slowly and the infinitive-order approximation of the CCSD(T) method is necessary.

One of the interesting problems we found during this study is the loss of electronic stability of AD^{2-} at the equilibrium C_{2h} geometry of AD^- (see Table 3). This suggests that, in some regions of the potential energy surface, the system with two excess electrons is not stable toward electron autodetachment. However, with the experimental conditions in mind, it is not likely that this would affect the observed PES because the dianions observed experimentally should consist primarily of near-D_{2d} species. Therefore, the region of potential energy surface where AD^{2-} is unstable is unlikely to be accessed experimentally.

For the sake of completeness, we also show in Table 3 the vertical electron binding energies for detaching an electron from the AD^- to produce neutral AD. For both geometries considered, the electronic stabilities of the monoanion are very large (∼5 eV).

5.3. Excited States of the AD^- Monoanion. The observed photoelectron spectra of AD^{2-} (Figure 1) contain several higher energy bands (A to D), which are due to removal of more tightly bound electrons and correspond to excited states of the AD^- monoanion. These bands are all very broad, probably due to vibrational excitations caused by geometry changes and/or possible overlapping electronic states. We undertook additional electronic structure calculations to estimate the energies of the first few excited electronic states of AD^-. In these calculations we used the equilibrium D_{2d} geometry of AD^{2-}, keeping in mind the vertical nature of all the photodetachment transitions.

We calculated the positions of the excited states of AD^- both directly (by using the OVGF method) and indirectly (by calculating CCSD(T) energies of the states of interest and subtracting them from the CCSD(T) ground-state energy of the dianion). Our results are given in Table 1 for several detachment channels along with the symmetries of the MOs from which the electron is removed and the final-state symmetries in the D_{2d} point group. We employed coupled-cluster CCSD(T) calculations on the first three excited states to try to achieve more reliable assignments. These results along with the CCSD(T) result for the ground state are also given in Table 1.

5.4. MP2 Geometries and Harmonic Frequencies of SD^{2-} and SD^-. The effort we undertook to study the electronic stability of SD^{2-} was motivated by the fact that this dianion was difficult to observe in our experiment. This observation

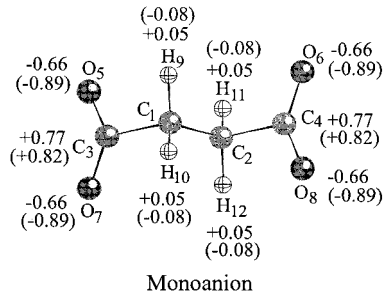

Figure 5. The minimum energy structure for $(O_2C-CH_2-CH_2-CO_2)^-$ at the C_{2h} symmetry. The numbers are the ep charges. The dianion has the same C_{2h} symmetry (Table 4) and its ep charges are given in parentheses.

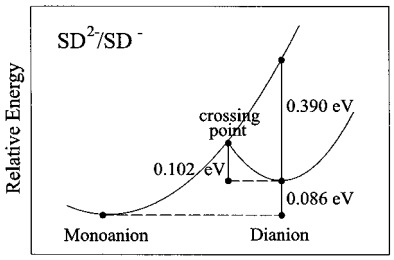

Figure 6. Schematic potential energy curves showing the relative energies for the mono- and dianion of the $(O_2C-CH_2-CH_2-CO_2)$ species. Note the minimum energy of the dianion is above that of the monoanion, suggesting that the dianion is not adiabatically electronically stable, but it is vertically electronically stable. The "cross point" defines a configuration, where the dianion and monoanion have identical electronic stability.

suggested that SD^{2-} might be electronically unstable, even though, as discussed earlier, chemical intuition suggests a similar separation of the two excess electrons in SD^{2-} and AD^{2-} and thus similar stabilities might be expected.

According to our MP2 calculations, both SD^{2-} and SD^- possess minima at C_{2h} symmetry (Figure 5) and as shown in Figure 6, these minima are spaced by 0.086 eV. The geometries of these two species are nearly identical and are shown in Figure 5 along with the charge distributions. Table 4 gives the details of the structural parameters and their vibrational frequencies. Attachment of an electron to the SD^- monoanion leads to small changes in bond lengths with the most significant being shortening of the C1−C3 bond by 0.108 Å (see Table 4). The shortening of the C1−C3 bond length is related to a bonding interaction between C1 and C3 in the highest occupied MO (HOMO) of SD^{2-}, as will be discussed later. Also, the valence angle $C_2C_1C_3$ increases by 5°, which causes the carbon skeleton to be more linear when two extra electrons are attached. However, the largest change we observe is in the $O_5C_3O_7$ valence angle, which decreases by 9° when the dianion is formed. Except for the slight decrease of the C1−C3 bond length in SD^{2-}, all the other structural changes reduce the Coulomb repulsion between the two excess charges in the dianion, as one would expect.

5.5. Electron Binding Energies of SD^{2-}. Our calculations carried out at various levels indicate that SD^{2-} is not electronically stable at the equilibrium geometry of the monoanion (see Table 5). However, it is stable at its own equilibrium geometry where our best estimation of the vertical detachment energy is 0.390 eV (0.475 eV with ZPE). As in the case of AD^{2-}, highly correlated ab initio methods have to be used to obtain correct values of the electron binding energy since the MP*n* results are inconclusive (Table 5). Our calculated adiabatic electron affinity of SD^- is −0.086 eV, meaning that SD^{2-} is adiabatically unstable with respect to electron loss. That is, SD^{2-} can be considered to be vertically electronically stable, but adiabatically electronically unstable. This conclusion is consistent with the experimental difficulty in observing this dianion from our ion source if vibrational motions of SD^{2-} cause it to sample geometries (near) where SD^{2-} is unstable relative to SD^-.

Since our calculations indicated that the dianion can be electronically stable at some geometries (relatively close to the C_{2h} dianionic minimum), we decided to find the geometry corresponding to the point where the potential energy surfaces for the mono- and dianion intersect. Our search, carried out at the CCSD(T) level, led us to a C_{2h} symmetry structure similar to that shown in Figure 5. The geometrical parameters of the crossing point gathered in Table 4 indicate that this structure is closer to the minimum obtained in Section 5.4 for the dianion than for the monoanion. The intersection of the SD^{2-} and SD^- energy surfaces is shown schematically in Figure 6, which also contains the relevant energetic information described in this section. Indeed, all the geometrical parameters defining the structure of the "crossing point" lie between the corresponding values calculated for the mono- and dianions at their minima. In every case, the values are closer to those for the dianionic structure.

6. Discussions

6.1. Molecular Orbitals of AD^{2-} and SD^{2-}: Charge Localization vs Delocalization. Figures 7 and 8 show the top few occupied MOs of AD^{2-} and SD^{2-}, respectively. It is instructive to compare the MOs of the two dianions and discuss their differences. Despite the fact that the carboxylate groups are the charge carriers in AD^{2-}, its (degenerate) HOMO contains a dominant portion of $-C\equiv C-$ π-bonding MOs with some contributions from the in-plane lone pairs of the O atoms. This suggests that the $-C\equiv C-$ π systems are strongly interacting with the terminal carboxylate groups. It is also interesting to observe that the C1−C2 bond length is nearly the same in AD^{2-} and AD^-, although clearly a π bonding electron is removed to form the monoanion. This suggests that there must be a strong relaxation effect upon the removal of the HOMO electron from AD^{2-}. The strong relaxation effect is shown most clearly from the binding energies given in Table 3 between the results at the KT and SCF levels. There is no relaxation effect included in the KT calculation, which overestimates the binding energy by more than 1.5 eV relative to the SCF value for AD^{2-}.

The HOMO-1 and HOMO-2 of AD^{2-} are pure O lone pair orbitals. However, the next three MO's all show some contributions from C1 and C2. The most interesting is HOMO-4, which consists of a degenerate set describing bonding interactions between the O lone pairs on each terminal carboxylate and the in-plane π-type MO of $-C\equiv C-$. This extra bonding interaction is likely the origin of the D_{2d} structure of AD^{2-} and provides the mechanism for slight charge delocalization from the terminal carboxylate groups.

In contrast, the MOs of SD^{2-} shown in Figure 8 indicate that the negative charges are almost completely localized on the terminal carboxylate groups. This is also consistent with the charge distributions given in Figure 5 for SD^{2-}. The HOMO of SD^{2-} has a significant contribution from the C1−C3 σ bond, which is consistent with the fact that the C1−C3 bond length is slightly shorter in SD^{2-} than in SD^- (Figure 5).

6.2. Assignments of the PES Features of AD^{2-}. On the basis of the Koopmans' approximation, the PES features in Figure 1 can be viewed as removing one electron from the dianion's occupied MOs (Figure 7) successively. However, the ordering

Table 4. MP2 Geometries and Vibrational Frequencies Calculated for the Dianion and Monoanion of ($O_2C-CH_2-CH_2-CO_2$) and for the Structure Corresponding to the Point on the Potential Energy Surface at Which They Intersect[a]

C_{2h} equilibrium structure of $(O_2C-CH_2-CH_2-CO_2)^{2-}$				
$r(C_1C_2) = 1.546$	$r(C_2C_4) = 1.555$	$r(C_3O_5) = 1.279$	$r(C_3O_7) = 1.279$	$r(C_1H_9) = 1.104$
$r(C_1H_{10}) = 1.104$	$\alpha(C_2C_1C_3) = 112.47$	$\alpha(O_5C_3O_7) = 126.66$	$\alpha(H_9C_1H_{10}) = 109.50$	$\gamma(H_9C_1H_{10}C_3) = 119.43$
$\nu_1(a_u) = 30$	$\nu_2(b_g) = 42$	$\nu_3(a_u) = 86$	$\nu_4(b_u) = 165$	$\nu_5(a_g) = 216$
$\nu_6(b_g) = 416$	$\nu_7(a_u) = 466$	$\nu_8(a_g) = 607$	$\nu_9(b_u) = 622$	$\nu_{10}(b_u) = 767$
$\nu_{11}(a_g) = 770$	$\nu_{12}(a_u) = 786$	$\nu_{13}(b_u) = 887$	$\nu_{14}(a_g) = 946$	$\nu_{15}(b_g) = 1011$
$\nu_{16}(a_g) = 1054$	$\nu_{17}(a_u) = 1130$	$\nu_{18}(b_u) = 1202$	$\nu_{19}(b_g) = 1273$	$\nu_{20}(a_g) = 1287$
$\nu_{21}(b_u) = 1350$	$\nu_{22}(a_g) = 1365$	$\nu_{23}(a_g) = 1450$	$\nu_{24}(b_u) = 1463$	$\nu_{25}(a_u) = 1573$
$\nu_{26}(b_g) = 1575$	$\nu_{27}(a_g) = 3043$	$\nu_{28}(b_u) = 3049$	$\nu_{29}(b_g) = 3099$	$\nu_{30}(a_u) = 3120$
C_{2h} equilibrium structure of $(O_2C-CH_2-CH_2-CO_2)^{-}$				
$r(C_1C_2) = 1.487$	$r(C_2C_4) = 1.663$	$r(C_3O_5) = 1.249$	$r(C_3O_7) = 1.249$	$r(C_1H_9) = 1.099$
$r(C_1H_{10}) = 1.099$	$\alpha(C_2C_1C_3) = 107.46$	$\alpha(O_5C_3O_7) = 135.82$	$\alpha(H_9C_1H_{10}) = 112.18$	$_g(H_9C_1H_{10}C_3) = 115.26$
$\nu_1(a_u) = 32$	$\nu_2(b_g) = 51$	$\nu_3(a_u) = 83$	$\nu_4(b_u) = 155$	$\nu_5(a_g) = 202$
$\nu_6(b_g) = 366$	$\nu_7(a_u) = 401$	$\nu_8(a_g) = 557$	$\nu_9(b_u) = 571$	$\nu_{10}(a_g) = 695$
$\nu_{11}(b_u) = 716$	$\nu_{12}(a_g) = 755$	$\nu_{13}(a_u) = 793$	$\nu_{14}(b_u) = 935$	$\nu_{15}(b_g) = 948$
$\nu_{16}(a_u) = 1097$	$\nu_{17}(a_g) = 1136$	$\nu_{18}(a_g) = 1153$	$\nu_{19}(b_u) = 1201$	$\nu_{20}(b_g) = 1268$
$\nu_{21}(a_g) = 1296$	$\nu_{22}(b_u) = 1463$	$\nu_{23}(a_g) = 1474$	$\nu_{24}(a_u) = 1726$	$\nu_{25}(b_g) = 1729$
$\nu_{26}(b_u) = 2766$	$\nu_{27}(a_g) = 3099$	$\nu_{28}(b_u) = 3158$	$\nu_{29}(b_g) = 3177$	$\nu_{30}(a_u) = 3198$
crossing point for $(O_2C-CH_2CH_2-CO_2)^{2-}/(O_2C-CH_2CH_2-CO_2)^{-}$				
$r(C_1C_2) = 1.517$	$r(C_2C_4) = 1.609$	$r(C_3O_5) = 1.264$	$r(C_3O_7) = 1.264$	$r(C_1H_9) = 1.102$
$r(C_1H_{10}) = 1.102$	$\alpha(C_2C_1C_3) = 110.80$	$\alpha(O_5C_3O_7) = 129.72$	$\alpha(H_9C_1H_{10}) = 110.63$	$\gamma(H_9C_1H_{10}C_3) = 118.14$

[a] Distances in Å, valence (α) and dihedral (γ) angles in deg, frequencies in cm^{-1}. See Figure 5 for atom numbering.

Table 5. Electron Binding Energies (eV) for the $(O_2C-CH_2-CH_2-CO_2)^{2-}$ Dianion

E	C_{2h} geometry of the dianion	C_{2h} geometry of the monoanion
E^{KT}	2.043	0.616
E^{SCF}	1.023	−0.498
E^{MP2}	−0.082	−0.995
E^{MP3}	0.709	−0.441
E^{MP4}	0.103	−0.882
$E^{CCSD(T)}$	0.390	−0.670
$E^{CCSD(T)} + \Delta ZPE$	0.475	−0.585

of the final states may be altered due to the strong electron relaxation effect, as discussed above. The vertical binding energies obtained using OVGF methods are given in Table 1. It is seen indeed that the final state ordering is different from the MO ordering. For the first four detachment channels, we also calculated the VDEs at the CCSD(T) level, which gave changes on the order of 0.3−0.5 eV. The VDE calculated for the ground state due to removal of an electron from the HOMO (e) of AD^{2-} is in excellent agreement with the measured VDE of 0.60 eV, although the zero-point-energy correction in fact worsens this agreement as shown in Table 3. The ^2E final state under D_{2d} symmetry is not stable due to Jahn−Teller effects and the equilibrium structure of AD^- is distorted to a lower symmetry (C_{2h}), as shown in Figure 3. The significant width of the X-band of the PES spectra (Figure 1) is in excellent agreement with the large geometry changes between AD^{2-} and AD^-. The first three excited states of AD^-, due to removal of an electron from the a_1, a_2, and b_1 MOs, are closely spaced, and should correspond to the A-band in the PES spectra. The VDEs at the CCSD(T) level agree very well with the average experimental VDE for the A-band.

We did not carry out CCSD(T) calculations for the more highly excited states of AD^-, for which only OVGF calculations were performed. However, on the basis of the discrepancies between the OVGF and CCSD(T) calculations for the first four states, we can still use these OVGF results to qualitatively assign the higher binding energy PES features. The next excited state from the OVGF calculations is the $^2B_2$ state due to removal of an electron from the b_2 MO and is ∼0.4 eV higher than the $^2B_1$ state. This state should correspond to the B-band. If we take into account an empirical −0.5 eV correction to the OVGF calculations, the VDE of the $^2B_2$ state would be in reasonable agreement with the VDE of the B-band at 1.70 eV. The next excited state is a degenerate ^2E state due to removal of an electron from HOMO-4 (Figure 7) with an OVGF VDE of 2.476

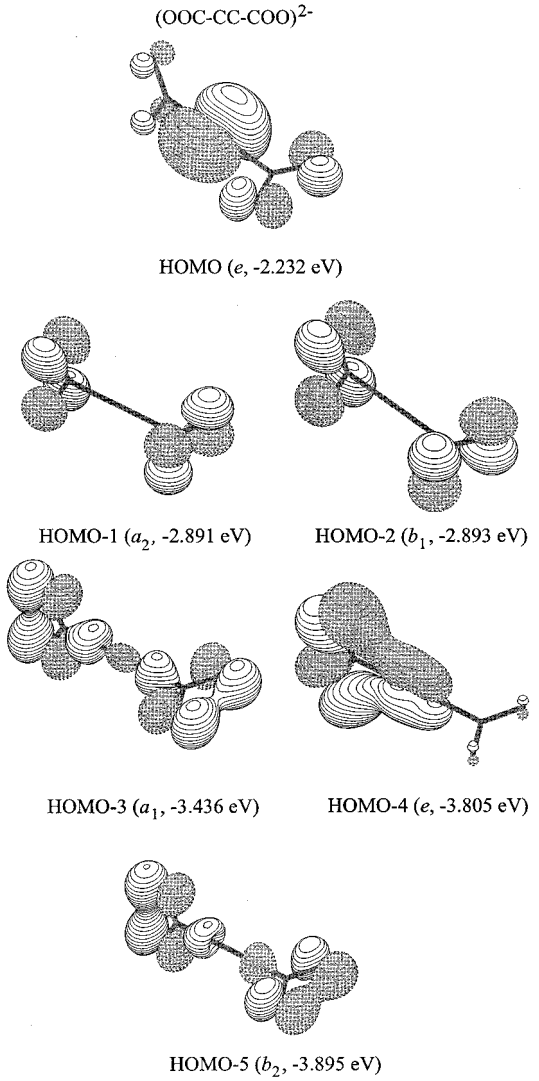

Figure 7. Molecular orbitals near the HOMO energy for the $(O_2C-C\equiv C-CO_2)^{2-}$ dianion. The MO symmetry and energy are given in parentheses.

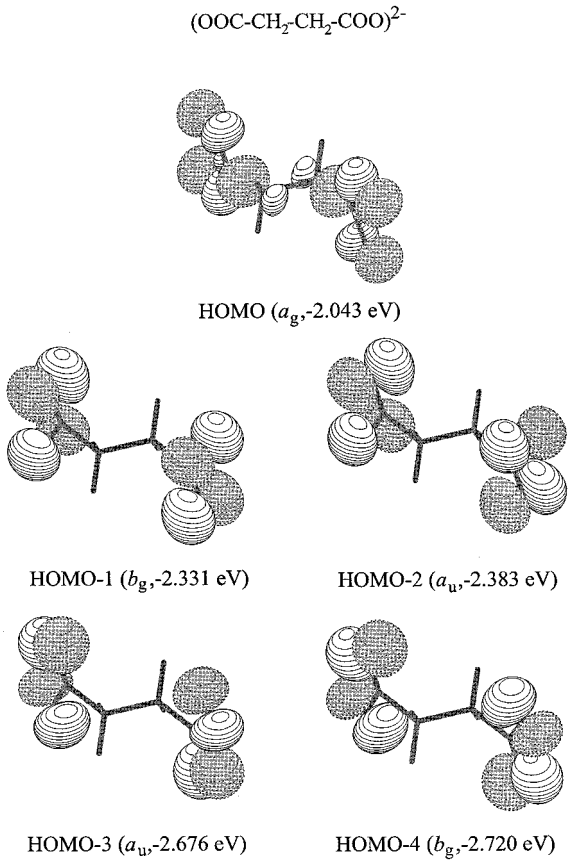

Figure 8. Molecular orbitals near the HOMO energy for the $(O_2C-CH_2-CH_2-CO_2)^{2-}$ dianion. The MO symmetry and energy are given in parentheses.

eV. The next excited state is again of ^{2}E symmetry, which is 3.5 eV higher and could not have been accessed in our experiment even with the expected correction of the OVGF VDE, because of the 3 eV RCB, which would cut off all features beyond about 3.5 eV at 193 nm (Figure 1c). Therefore, we tentatively assign the C and D bands to be due to the removal of an electron from HOMO-4. The resulting ^{2}E state is again unstable due to the Jahn−Teller effect and is conceivably split to yield the two PES bands.

6.3. Origins of the Relative Stabilities of AD^{2-} and SD^{2-}. According to our previous studies,[21,22] the RCB in a dianion is equal to the magnitude of the intramolecular Coulomb repulsion between the two excess charges (when these charges are clearly localized). For a dianion to be stable electronically in the gas phase, its second electron binding capability must exceed the Coulomb repulsion. Thus the electronic stability of a dianion is determined by two factors: (1) the magnitude of the intramolecular Coulomb repulsion due to the two excess charges, and (2) the potential for binding a second electron by the monoanion. The first factor is determined by the size and structure of the molecule. The second factor depends on the specific character of the lowest available valence orbital of the anion as well as the associated neighboring groups. For MCAs, there is also an additional issue of thermodynamic stability relative to charge-separation fragmentation. For a MCA to be thermodynamically stable relative to such fragmentation, the chemical bonding must also be strong enough to overcome the Coulomb repulsion. As we have recently discussed,[28] both the electronic and thermodynamic stabilities are important for the observability of a free dianion. For the current dianions, AD^{2-} and SD^{2-}, they are both thermodynamically stable relative to fragmentation due to the strong C−C bond strength. It is the electronic stability that therefore is likely to limit their laboratory observations.

Since the charge carriers in AD^{2-} and SD^{2-} are the same, the difference in their electronic stability must lie in their detailed structural difference and in the intervening CH_2CH_2 and C≡C moieties. From the optimized structures of AD^{2-} and SD^{2-}, we can roughly estimate their intramolecular Coulomb repulsion by assuming that the charges are localized on the O atoms (which is more true in SD^{2-} than in AD^{2-}). The O−O distance (R) in AD^{2-} is 5.61 Å, giving a Coulomb repulsion of 2.6 eV (e^2/R), which is fairly close to our estimated RCB of ∼3 eV. The fact that the simple estimate using the O−O distance and Coulomb's law is smaller than the experimentally estimated RCB in AD^{2-} is an indication of charge delocalization, which tends to increase the Coulomb repulsion term in this case. There are two types of O−O distance in SD^{2-} (O5−O6 = 5.05 Å, O5−O8 = 5.54 Å). Using the average O−O distance, we obtain a Coulomb repulsion of 2.7 eV, which is quite close to the simple estimate for that of AD^{2-}, consistent with our original notion that AD^{2-} and SD^{2-} should have similar electronic stability on the basis of their similar molecular sizes.

The favored stability of AD^{2-} over SD^{2-} must then be due to the −CC− triple bond that enhances the potential of AD^- to bind a second electron. This is shown most clearly in the MO pictures in Figures 7 and 8. While the carboxylates in SD^{2-} are fairly localized, those of AD^{2-} have significant interactions with the −CC− moiety. In particular, the two MOs of HOMO-4 in AD^{2-} provide a mechanism for the extra stabilization of the excess charges by delocalization. The charge distributions shown in Figure 3 are consistent with this picture. We then suggest that there is a combination of charge delocalization in AD^{2-} and extra Coulomb repulsion that disfavors delocalization. In the D_{2d} symmetry, the AD^{2-} dianion is apparently able to take advantage of the extra stabilization through delocalization while minimizing the additional Coulomb repulsion. This is most likely the origin why AD^{2-} is more stable than SD^{2-}. The results shown in Table 3 and Figure 4 unequivocally support this conclusion because, at D_{2d} symmetry, AD^{2-} is electronically unstable relative to the C_{2h} monoanion. The influence of the −C≡C− triple bond on the stability of the molecules can also be seen in the electron binding energies of the monoanions. The AD^- anion has a VDE of 4.967 eV from our CCSD(T) calculation (Table 3), whereas the SD^- anion only has a VDE of 4.632 eV.

Finally we wish to comment on the experimental observability of metastable MCAs and their lifetimes. Because of the expected RCB, SD^{2-} should still be electronically metastable with a finite lifetime. In fact, SD^{2-} had been observed previously in a collisionally induced "ion-pair" formation experiment along with other $^-OOC-(CH_2)_n-COO^-$ dianions.[31] We have also observed the existence of SD^{2-} in our experiment, though with extremely weak abundance, consistent with its metastability. On the basis of our experimental time scale, we estimated that the lifetime of SD^{2-} must be less than 0.1 s under our experimental conditions. Indeed, we have observed previously abundant metastable MCAs with longer lifetimes.[27−30]

7. Conclusions

We have performed a comprehensive experimental and theoretical study on two small gaseous dicarboxylate dianions, acetylene dicarboxylate and succinate. Contrary to our initial chemical intuition, they show very different gas-phase stability with respect to electron loss. We were able to produce abundant AD^{2-} dianions with our electrospray ion source and were able

to measure its photodetachment spectra. We determined its adiabatic electron binding energy to be 0.30 (0.10) eV. Our theoretical study predicts that AD^{2-} is adiabatically and vertically electronically stable by 0.42 and 0.69 eV, respectively. The calculated vertical binding energies for various detachment channels also allowed us to assign the detachment features. We found that AD^{2-} has a D_{2d} structure and undergoes a major Jahn−Teller distortion as the ground-state AD^- monoanion is formed. The significant geometry changes between AD^{2-} and AD^- agree well with the broad photodetachment feature observed. On the other hand, our calculations predict that SD^{2-} is electronically adiabatically unstable, although it is vertically electronically stable. Moreover, it is likely that vibrational motions of SD^{2-} cause geometries to be reached where SD^{2-} is electronically unstable. This is consistent with our experimental difficulty to observe it in the gas phase. The origin of the stability difference in AD^{2-} and SD^{2-} is suggested to be due to significant interactions between the carboxylate groups and the −CC− triple bond system in AD^{2-} that allows slight charge delocalization into the π-type MOs while minimizing the Coulomb repulsion under the D_{2d} symmetry.

Acknowledgment. The theoretical work done in Utah is supported by the National Science Foundation (CHE-9618904). The authors acknowledge the Center for High Performance Computations at the University of Utah for computer time. L.S.W. wishes to thank Dr. Michel Dupuis for valuable discussions. The experimental work done in Washington is supported by The U.S. Department of Energy, Office of Basic Energy Sciences, Chemical Science Division. Acknowledgment is also made to the donors of the Petroleum Research Fund, administered by the American Chemical Society, for partial support of this research (to L.S.W.). The experiment was performed at the W. R. Wiley Environmental Molecular Sciences Laboratory, a national scientific user facility sponsored by the Department of Energy's Office of Biological and Environmental Research and located at Pacific Northwest National Laboratory. Pacific Northwest National Laboratory is operated for the U.S. Department of Energy by Battelle. L.S.W. is an Alfred P. Sloan Foundation Research Fellow.

JA000371F